

# Experimental observation of hydrodynamic-like behavior in 3D topological semimetal $\text{ZrTe}_5$

Chang-woo Cho<sup>a,b</sup>, Peipei Wang<sup>a</sup>, Fangdong Tang<sup>a</sup>, Sungkyun Park<sup>b</sup>, Mingquan He<sup>c</sup>, Rolf Lortz<sup>d</sup>, Genda Gu<sup>e</sup>, Qiang Li<sup>e,f</sup>, and Liyuan Zhang<sup>a,\*</sup>

<sup>a</sup>*Department of Physics, Southern University of Science and Technology, Shenzhen 518055, China*

<sup>b</sup>*Department of Physics, Pusan National University, Busan 46241, South Korea*

<sup>c</sup>*Low Temperature Physics Lab, College of Physics & Center of Quantum Materials and Devices, Chongqing University, Chongqing 401331, China*

<sup>d</sup>*Department of Physics, The Hong Kong University of Science and Technology, Clear Water Bay, Kowloon, Hong Kong*

<sup>e</sup>*Condensed Matter Physics and Materials Science Department, Brookhaven National Laboratory, Upton, NY 11973, USA*

<sup>f</sup>*Department of Physics and Astronomy, Stony Brook University, Stony Brook, New York 11794-3800, USA*

\*corresponding author: Liyuan Zhang

**Email:** zhangly@sustech.edu.cn

**Author Contributions:** This work was initiated by L.Z.; C.w.C. carried out the electrical and thermal transport measurements with help of P.W., F.T., M.H. and R.L.; the single crystal samples were provided by G.G. and Q.L.; C.w.C., P.W. and L.Z. analyzed the data with the help of S.P., M.H. and R.L.; the manuscript was prepared by C.w.C. and L.Z. with the help of S.P. and R.L., and all authors were involved in discussions and contributed to the manuscript.

**Competing Interest Statement:** The authors declare no competing interest.

**Classification:** condensed matter physics, topological semimetal

**Keywords:** hydrodynamics, thermal conductivity, phonon, thermal Hall effect

## Abstract

Hydrodynamic fluidity in condensed matter physics has been experimentally demonstrated only in a limited number of compounds due to the stringent conditions that must be met. Herein, we demonstrate phonon hydrodynamic-like properties in three-dimensional topological semimetal  $\text{ZrTe}_5$  thanks to its ultrahigh-purity and intrinsic structural instability. By measuring the thermal properties in a wide temperature range, two representative experimental evidences of the hydrodynamics are seen in an interesting temperature window between the ballistic and diffusive regimes: a faster evolution of the thermal conductivity than in the ballistic regime and the non-monotonic temperature-dependent effective quasiparticle mean-free-path. In addition, magneto-thermal conductivity results indicate us that charged quasiparticles, as well as phonons, may also play an important role in the hydrodynamic flow in  $\text{ZrTe}_5$ .

## Significance Statement

Strongly correlated interparticle scattering such as hydrodynamics is the forefront of physics research in recent years. Renewed attention in hydrodynamics of correlated systems stems from the heavy-ion collisions and transport experiments in condensed matter. In the case of condensed matter semimetals, extraordinary interactions have been reported, but those are in either electron or phonon viscosity flow almost exclusively. In this study, we provide transport evidence of weakly coupled hydrodynamics between phonons and charged quasiparticles in three-dimensional topological semimetal  $\text{ZrTe}_5$  as thickness is reduced. This work breaks ground for understanding and manipulating unconventional heat flow in three-dimensional topological materials.

## Main Text

### Introduction

In insulators, heat is mainly carried by phonons. This phonon-dominant heat conduction is described by Fourier's law, in which phonons scatter from other phonons, impurities, and boundaries (1-3). This process takes place through the momentum-relaxing process known as Umklapp scattering (U-scattering). During this process, heat fluxes are dissipated and the crystal momentum is not conserved (1-3). On the other hand, at a sufficiently low temperature  $T$ , Fourier's law no longer holds, where the crystal momentum is conserved thanks to the dominant Normal scattering (N-scattering) (4-6). These two types of scattering mechanisms are known for a diffusive and a ballistic regime, respectively, and have been widely studied in many solids (7-11).

Meanwhile, Gurzhi proposed a viscous flow driven by the heat carriers when N-scattering is abundant in the overlapping two regimes (12). Since then, it has been called hydrodynamic flow due to its analogy with macroscopic transport phenomena in water fluids. (13). In the case where phonons represent the primary heat carriers in solids, two significant characteristics are known as Poiseuille flow and the second-sound wave (6, 14). The former is characterized by a steady-state phonon flow in which thermal resistance diffuses due to the boundary scattering combined with N-scattering (15, 16). In comparison, the latter involves wave-propagation of a  $T$ -gradient without significant attenuation (6, 17, 18).

Despite the fascination of phonon-hydrodynamics (PH) in solid state systems, experimental observation is rare. Moreover, it is found only in a narrow  $T$ -window at a remarkably low  $T$ , where

abundant N-scattering and a suitable sample size are additionally required. For instance, the reported  $T$ -window of Poiseuille flow in suspended graphene was only 0.5 K at about 1 K. (19). One reason for this practical difficulty is that U-scattering overwhelms N-scattering in almost every  $T$ -range except at significantly low  $T$ . For these reasons, PH behavior has been experimentally confirmed in only a handful of compounds, such as solid He<sup>3</sup> (20) and He<sup>4</sup> (21), Bi (22), black P (16) and SrTiO<sub>3</sub> (23). Therefore, the search for new materials in which hydrodynamics contributed through phonons or other collective excitations is of great interest to the condensed matter community.

In this study, we performed thermal and electrical transport experiments for topological semimetal ZrTe<sub>5</sub> to investigate the hydrodynamic property. In fact, the ZrTe<sub>5</sub> study is initiated decades ago due to its considerable thermoelectric performance and resistivity anomaly (24, 25). Recently, it has gained renewed attention due to non-trivial topological phenomena such as a 3D quantum Hall effect (26), a quantum spin Hall effect on a monolayer (27), and a chiral magnetic effect (28). Moreover, it has been reported that bulk ZrTe<sub>5</sub> sits at the boundary between a weak- and a strong-topological phase, so that an external perturbation easily affects its topology (29-31). Herein, we present experimental evidence for PH by observing a faster evolution of the thermal conductivity  $\kappa$  than in the ballistic regime. In contrast to the conventional PH, we find an unexpected thermal transport behavior in a hydrodynamic regime, which could be attributed to the charged quasiparticles. After reviewing several scenarios, we suggest that hydrodynamic flow is led by mainly phonons, but weakly coupled to charged quasiparticles. Our findings have important implications for ongoing research on the various possible types of hydrodynamics, especially in a three-dimensional topological semimetal.

## Results

In the following, we will examine the first evidence of hydrodynamic flow. In a PH regime,  $\kappa$  should evolve faster than a  $T^3$ -dependence. To test this, we plot the  $T$ -dependent total thermal conductivity  $\kappa_{tot}$  in the ZrTe<sub>5</sub> single crystals, which are shown in **Fig. 1a**. The detailed samples information and their electrical property are noted in the method section and supplementary **Fig. S4**, respectively. The electronic contribution of thermal conductivity  $\kappa_{WF}$  (solid lines) is presented in **Fig. 1b**. Note that only  $\kappa_{tot}$  is a directly measured value, whereas  $\kappa_{WF}$  is extracted from the Wiedemann-Franz (WF) law ( $\kappa_{WF} = \frac{T}{\rho} L_0$ , Lorenz number  $L_0 = 2.44 \times 10^{-8} \text{ W}\Omega\text{K}^{-2}$ ) based on our electrical resistivity data. For clarity, it is plotted on a log-log scale here. In the high  $T$ -regime ( $\sim 200$ - $300$  K in Sample#1, and  $\sim 30$  -  $300$  K in Sample#2 and #3), it follows nearly  $1/T$  dependence in all the samples, meaning that the U-scattering is the most prominent process in this range. After passing through the  $\kappa_{tot}$  peak, it starts to decrease, indicating the N-scattering process begins to dominate. In the case of our thickest sample (#1,  $t = 0.3 \text{ mm}$ ), we do not observe any hydrodynamic features here. While Sample#2 and #3 show anomalous thermal transport behavior near the hydrodynamic regime. In Sample#3 ( $t = 0.2 \text{ mm}$ ), it first shows a downward kink-like anomaly just below the  $T$  where the maximum occurs. With further cooling, the slope of  $\kappa_{tot}$  gradually increases towards low  $T$  and exceeds a  $T^3$ -dependence (dashed line in **Fig. 1a**) in a range of 0.8 to 2.0 K. In the case of the thinnest sample (#2,  $t = 0.1 \text{ mm}$ ), it is much clear that a faster evolution regime rather than  $T^3$ -dependence. It should be mentioned that, if  $\kappa_{tot}$  assumes the summation of phononic and electronic contribution, in this study the phonon thermal conductivity  $\kappa_{ph}$  dominates by more than

one order of magnitude across the entire  $T$ -range. In addition, the  $\kappa_{tot}$  must converge to  $\kappa_{WF}$  at sufficiently low  $T$ , since the thermal energy at low  $T$  is mainly transferred from the charge carriers. However, we see no convergence up to the experimental low  $T$ -limit of 0.7 K. This is due to the comparatively high-purity crystallinity and extremely low carrier density at low  $T$  (see **Fig. S4b and c**), so that phonons still play a crucial role at low  $T$ . We thus deduce that such a hydrodynamic feature is attributed to dominant phonons in this system.

Next, we examine the magnetic-field dependence of thermal transport. In **Fig. 2a**, we present the longitudinal thermal conductivity  $\kappa_{xx}$  as a function of  $B$ -field in Sample#3, which measured at  $T = 0.81$  K. For comparison with the electronic contribution, we plot together with  $\kappa_{WF}$  (red solid line in **Fig. 2a**) measured at  $T = 0.70$  K. Two things are worth noting here. First, one sees an apparent thermal quantum oscillation that is in complete agreement with the electronic quantum oscillations. Although phonons still play a dominant role up to our experimental low- $T$  limit of 0.7 K, it means that the contribution of charged particles among thermal carriers increases when  $T$  is lower. Second, it hardly responds to  $\kappa_{xx}$  when the external  $B$ -fields are sufficiently high. When the quantum oscillations terminate at  $\sim 1.5$  T,  $\kappa_{xx}$  is nearly constant in a higher field regime. We also confirm this for Sample#2 that  $\kappa_{xx}$  is less sensitive to the  $B$ -fields regardless of base  $T$  (see **Fig. S5**).

An unexpected thing is seen in the  $T$ -dependent electronic thermal contribution. In general, it is known that  $\kappa_{ph}$  does not seriously change by the external  $B$ -fields, thus we may extract the thermal contribution of charged quasiparticles by subtracting the  $\kappa_{xx}(B)$  from the  $\kappa_{xx}(0T)$ . To do this, we define  $\Delta\kappa = \kappa_{xx}(0T) - \kappa_{xx}(B)$  and plotted in **Fig. 2b**, where the magnitude of  $B$ -field was chosen to be 2.4 T and 5.0 T for Sample#3 and #2, respectively. Surprisingly, this quantity exhibits a distinct deviation in the hydrodynamic window we observed.

To gain a deeper understanding, we carry out the thermal Hall experiment, as this could be a direct probe to study quasiparticle dynamics, but has rarely been performed in topological materials due to the difficulty of obtaining high-quality data. **Figure 3a** shows the  $B$ -field dependence of the thermal Hall resistivity  $\omega_{xy}$  ( $= \frac{wt}{l} \left( \frac{\Delta T_{xy}}{P} \right)$ , where  $\Delta T_{xy}$  and  $P$  denote the  $T$ -gradient between two points along the transverse direction and the heating power, respectively) in a narrow  $B$ -field range from -1 to 1 T. For a higher resolution, we recorded the data this time with a continuous field sweep mode. In the main text, only the case of Sample#2 is shown (The results of Sample#3 are included in supplementary **Fig. S6**). The  $\omega_{xy}$  is negligibly small in almost all  $B$ -fields except for in a very weak field region ( $|B| < 0.1$  T). It is noted that purely phononic thermal contribution cannot be detected by the thermal Hall signal due to its charge neutrality. Thus, zero thermal Hall voltage is acceptable because phonons are the primary heat carriers in ZrTe<sub>5</sub> single crystals in this study. Then, the transverse thermal gradient should not be generated under the  $B$ -fields. Interestingly, an asymmetric thermal Hall feature is found in a weak field region, it becomes stronger as  $T$  decrease.

The degree of heat deviation can be determined from the thermal Hall angle  $\tan \theta_H$ . In **Fig. 3b**,  $\tan \theta_H$  ( $= \frac{\kappa_{xy}}{\kappa_{xx}}$ ) is plotted as a function of  $B$ -field with various  $T$ . The trend is not different from  $\omega_{xy}$  versus  $B$ . It shows a significant deviation when the  $B$ -field is applied near zero-field and is abruptly faded in the region of higher  $B$ -fields. In **Fig. 3c**, we represent the zero-field-limit ( $B \rightarrow 0$ ) of  $\tan \theta_H / B$  (hereafter  $[\tan \theta_H / B]_0$ ), which is proportional to the effective mean-free-path of the quasiparticles  $l_{QP}$  (32). The magnitude of  $l_{QP}$  can be estimated through the equation  $l_{QP} =$

$\frac{\hbar k_F \tan \theta_H}{e B}$ , where  $\hbar$  is the Planck constant,  $k_F$  is the Fermi wave number, and  $e$  is the electron charge (33). Using the estimation of  $k_F \approx 4 \times 10^{-3} \text{ \AA}^{-1}$  in the *ac*-plane (26), we obtain that the  $l_{QP}$  is about 40  $\mu\text{m}$  at 1.0 K in both samples (#2 and #3), which is notably longer than those previously reported (34-36). This consequence also supports our extremely clean ZrTe<sub>5</sub> samples, so that quasiparticles travel without significant momentum loss. In particular, the  $l_{QP}$  is longer by a factor of 5 at about 0.7 K, where its length scale is comparable to our thinnest sample thickness (#2,  $t = 0.1 \text{ mm}$ ). Another striking feature of  $[\tan \theta_H / B]_0$  is the presence of a local maximum (vertical arrows in Fig. 3c) corresponding to  $T$  at  $\sim 1.8 \text{ K}$  (Sample #2) and  $\sim 2.2 \text{ K}$  (Sample #3), which presumably can be an additional signature of hydrodynamic flow. These are also in good agreement with the phonon-dominant hydrodynamic regime we observed.

## Discussion

So far, we have shown the hydrodynamic-like features from the thermal transport experiments. The question that arises from our results is how phonon-dominant hydrodynamics could be realized in the semimetallic ZrTe<sub>5</sub> and not in an insulator. In terms of the scattering time scale, the U-scattering time grows exponentially as decreasing  $T$ , while the N-scattering time is given by a power law  $T$ -dependence. The boundary scattering time must lie between the two for the realization of hydrodynamic flow. Not only are these conditions hardly satisfied intrinsically, but they are also easily affected by impurities. For this reason, the hydrodynamic regime is extremely fragile and has been found in a limited number of compounds with very narrow  $T$ -windows, so that it requires high-purity crystallinity. On the one hand, it is also pointing out that instability of the crystal structure may increase the stability of PH by enhancing N-scattering (37, 38). The materials in which a PH was reported, such as Bi, black P, and SrTiO<sub>3</sub>, are the supporting examples, because these were not ultra-pure systems like pure silicon. Since ZrTe<sub>5</sub> has been reported to have an unstable crystal structure and topology, its physical properties can be easily tuned by changing the growth environment and other external parameters (26, 30, 31). Therefore, the combination of relatively high-purity crystallinity and structural instability makes ZrTe<sub>5</sub> a perfectly suitable material to observe the phonon-dominant hydrodynamics.

Then it is puzzling what kind of collective quasiparticles induces the hydrodynamic flow in our case. Again, the thermal Hall signal is essentially from the electronic contribution, since the neutrally charged quasiparticles are not affected by a magnetic field. Therefore, it is reasonable to say that the hydrodynamic flow in ZrTe<sub>5</sub> is unlikely to be due to a purely phononic attribution. Although we demonstrate that the heat in ZrTe<sub>5</sub> is dominantly carried by the phonons, the electron-electron hydrodynamic scenario is still valid. In the results of the zero-field-limit electronic Hall-angle ( $[\tan \theta_e / B]_0$ , inset of Fig. 3c), we can test it. It increases steadily as  $T$  drops to  $\sim 10 \text{ K}$ , and then nearly saturates at low  $T$ . This indicates that the electron-electron scattering process below 10 K is virtually unaffected by the entire scattering system. From this, we may rule out the pure electron-electron fluid scenario.

The next possibility is an electron-phonon fluid in which the electron-phonon scattering process is the fastest, so that their momentum can be quasi-conserved. For electron-phonon cases studied previously, the results resembled ours to some extent, since there is a large violation of  $L/L_0$  (39). However, the sign of  $L/L_0$  is at odds with the present results as shown in Fig. 4, implying that our

system is much closer to a PH-like fluid. Moreover, we find no experimental evidence of the strong phonon-drag effect as they have reported.

Dirac fluid can be another candidate. According to the previous work of Crossno et al., in which they reported on a deviation of  $\kappa_{WF}$  with largely violated the  $L/L_0$  at a charge neutrality point in graphene, and they argued that this is indicative of Dirac fluid (40). Although seemingly similar to the present results (significant violation of  $L/L_0$  and nearly charge-neutrality point), our observations are different in principle. In the case of Crossno et al., the Dirac fluid hydrodynamics occurred in the non-degenerate regime (40), but our ZrTe<sub>5</sub> is far away in the degenerate regime. Furthermore, they observed a recovery of  $L/L_0$  as one moves away from the neutral point (40), but we see no recovery over the entire  $T$ -window in Sample#2 and #3 showing the hydrodynamic features. Given that none of the scenarios are likely to dominate the hydrodynamics in the present results, therefore we cautiously suggest that predominant PH flow that weakly coupled to charged quasiparticles in our three-dimensional topological semimetal ZrTe<sub>5</sub> crystals.

## Summary

In summary, the main effort of hydrodynamic studies to date has been to find the significant features where either electrons or phonons provide the primary scattering. However, all transport regimes – ballistic, hydrodynamic, and diffusive – can coexist and be coupled, making it difficult to distinguish purely quasiparticle hydrodynamic phenomena. Using ultrahigh-purity single crystals of ZrTe<sub>5</sub>, we have succeeded in finding the Hallmarks of the PH as well as the anomalous flow of charged quasiparticles, which is certainly unexpected. This requires extended theoretical and experimental work beyond the scope of the present study.

## Materials and Methods

In the experimental setup, we used ultrahigh quality ZrTe<sub>5</sub> single crystals, which were grown by the tellurium flux method. Thanks to the relatively large size of the single acicular crystals ( $l \times w \times t$ ; Sample#1: 3.0 x 0.4 x 0.3 mm<sup>3</sup>, Sample#2: 3.2 x 0.3 x 0.1 mm<sup>3</sup>, Sample#3: 2.9 x 0.3 x 0.2 mm<sup>3</sup>), we were able to perform the electrical and thermal transport experiments on the same bulk samples. Details of the sample growth and structural properties can be found elsewhere (26, 41, 42). In the main text, we defined the longest (shortest) dimension as along the  $a$ -axis ( $b$ -axis), corresponding to the ZrTe<sub>3</sub> chain (stacking layer) direction.

In the transport experiments, we performed the electrical resistivity measurements by the standard Hall bar method, using an alternating current with an amplitude of 0.01-0.1 mA and a frequency of 10-20 Hz. The magnetic field  $B$  was applied in the perpendicular direction to the  $ac$ -plane. In order to measure the thermal transport of such a needle-shaped ZrTe<sub>5</sub> crystal, we used a well-known steady-state method with one-heater and three-thermometers as shown in supplementary Fig. S1a-c. One end of a ~3.0 mm long sample was attached to a copper heat sink, while a small chip-like ~100 Ohm resistor and three well-calibrated Cernox thermometers were suspended from glass fibers. To minimize heat loss, thin Pt/W wires (25  $\mu$ m) were used between all electrical devices and electrodes on the holder, while thick Ag wires (100  $\mu$ m) were connected to the sample for the best thermal equilibrium state during the measurement. To eliminate spurious longitudinal (or

transverse) components, we measured and averaged every transport experiment in opposite  $B$ -field directions. In order to further calibration, we also measured the thermal conductivity of high-purity brass with this setup and calibrated it accordingly (see Supplementary **Fig. S2**). Since the sensitivity of the thermometers used in this study vanishes towards higher  $T$ , we switched to a thermocouple method to record the thermal gradient in the high  $T$  regime ( $T > \sim 20$  K). In the overlapping range (about 10-20 K), we confirmed the consistent  $\kappa$  results within the error bars; an example for Sample #3 is presented in supplementary **Fig. S3**.

## Acknowledgments

We thank Benjamin Piot and Kitinan Pongsangangan for their enlightening discussions. C.-w. Cho is supported by BK4-program from NRF-Korea. M. He acknowledges the support by National Natural Science Foundation of China (11904040), Chongqing Research Program of Basic Research and Frontier Technology, China (Grant No. cstc2020jcyj-msxmX0263), Fundamental Research Funds for the Central Universities, China (2020CDJQY-A056, 2020CDJ-LHZZ-010, 2020CDJQY-Z006), Projects of President Foundation of Chongqing University, China (2019CDXZWL002). The work at Brookhaven National Laboratory was supported by the U.S. Department of Energy (DOE) the Office of Basic Energy Sciences, Materials Sciences and Engineering Division under Contract No. DE-SC0012704.

## References

1. S. R. Phillpot, A. J. H. McGaughey, Introduction to thermal transport. *Materials Today* **8** (6), 18-20 (2005).
2. M. Kaviany, *Principles of Heat Transfer* (Wiley, New York, 2002).
3. J. M. Ziman, *Electrons and Phonons: The Theory of Transport Phenomena in Solids* (Oxford Univ. Press, 2001).
4. M. S. Dresselhaus *et al.*, New Directions for Low-Dimensional Thermoelectric Materials. *Adv. Mater.* **19**, 1043-1053 (2007).
5. W. J. De Haas, T. Biermasz, The thermal conductivity of KBr, KCl and SiO<sub>2</sub> at low temperatures. *Physica* **4**, 752-756 (1937).
6. C. C. Ackerman, B. Bertman, H. A. Fairbank, R. A. Guyer, Second Sound in Solid Helium. *Physical Review Letters* **16**, 789-791 (1966).
7. M. Maldovan, Transition between ballistic and diffusive heat transport regimes in silicon materials. *Applied Physics Letters* **101**, 113110 (2012).
8. J. Sirker, R. G. Pereira, I. Affleck, Diffusion and Ballistic Transport in One-Dimensional Quantum Systems. *Physical Review Letters* **103**, 216602 (2009).
9. J. S. Kang, M. Li, H. Wu, H. Nguyen, Y. Hu, Experimental observation of high thermal conductivity in boron arsenide. *Science* **361**, 575-578 (2018).
10. M. Koch, F. Ample, C. Joachim, L. Grill, Voltage-dependent conductance of a single graphene nanoribbon. *Nature Nanotechnology* **7**, 713-717 (2012).
11. H. M. Pastawski, Classical and quantum transport from generalized Landauer-Buttiker equations. *Physical Review B* **44**, 6329-6339 (1991).
12. R. N. Gurzhi, HYDRODYNAMIC EFFECTS IN SOLIDS AT LOW TEMPAB. *Soviet Physics Uspekhi* **11**, 255-270 (1968).

13. J. A. Sussmann, A. Thellung, Thermal Conductivity of Perfect Dielectric Crystals in the Absence of Umklapp Processes. *Proc. Phys. Soc.* **81**, 1122 (1963).
14. A. Cepellotti *et al.*, Phonon hydrodynamics in two-dimensional materials. *Nat. Commun.* **6**, 6400 (2015).
15. R. Maynard, A. Smontara, J. C. Lasjaunias, On the phonon Poiseuille flow in quasi-one dimensional crystal. *Physica B: Condensed Matter* **263-264**, 678-682 (1999).
16. Y. Machida *et al.*, Observation of Poiseuille flow of phonons in black phosphorus. *Sci. Adv.* **4**, eaat3374 (2018).
17. D. W. Pohl, V. Irniger, Observation of Second Sound in NaF by Means of Light Scattering. *Physical Review Letters* **36**, 480-483 (1976).
18. A. Koreeda, R. Takano, S. Saikan, Second Sound in  $\text{SrTiO}_3$ . *Physical Review Letters* **99**, 265502 (2007).
19. S. Lee, D. Broido, K. Esfarjani, G. Chen, Hydrodynamic phonon transport in suspended graphene. *Nat. Commun.* **6**, 6290 (2015).
20. W. C. Thomlinson, Evidence for Anomalous Phonon Excitations in Solid  $\text{He}^3$ . *Physical Review Letters* **23**, 1330-1332 (1969).
21. L. P. Mezhov-Deglin, Influence of Dimensions on the thermal conductivity of Crystalline He4 samples. *Soviet Physics JETP* **25**, 568-571 (1967).
22. V. N. Kopylov, L. P. Mezhov-Deglin, Investigation of the kinetic coefficients of bismuth at helium temperatures. *Zh. Eksp. Teor. Fiz.* **65**, 720-734 (1973).
23. V. Martelli, J. L. Jimenez, M. Continentino, E. Baggio-Saitovitch, K. Behnia, Thermal Transport and Phonon Hydrodynamics in Strontium Titanate. *Phys. Rev. Lett.* **120**, 125901 (2018).
24. S. Okada, T. Sambongi, M. Ido, Giant Resistivity Anomaly in ZrTe5. *Journal of the Physical Society of Japan* **49**, 839-840 (1980).
25. F. J. DiSalvo, R. M. Fleming, J. V. Waszczak, Possible phase transition in the quasi-one-dimensional materials ZrTe5 or HfTe5. *Physical Review B* **24**, 2935-2939 (1981).
26. F. Tang *et al.*, Three-dimensional quantum Hall effect and metal-insulator transition in ZrTe5. *Nature* **569**, 537 (2019).
27. H. Weng, X. Dai, Z. Fang, Transition-metal pentatelluride ZrTe5 and HfTe5: a paradigm for large-gap quantum spin Hall insulators. *Phys. Rev. X* **4**, 011002 (2014).
28. L. Y. Xiang *et al.*, Observation of non-Fermi liquid behavior in hole-doped LiFe1-xVxAs. *Phys. Rev. B* **94**, 094524 (2016).
29. Z. Fan, Q.-F. Liang, Y. B. Chen, S.-H. Yao, J. Zhou, Transition between strong and weak topological insulator in ZrTe5 and HfTe5. *Sci. Rep.* **7** (2017).
30. J. Mutch *et al.*, Evidence for a strain-tuned topological phase transition in ZrTe5. *Sci. Adv.* **5** (2019).
31. B. Xu *et al.*, Temperature-Driven Topological Phase Transition and Intermediate Dirac Semimetal Phase in ZrTe5. *Physical Review Letters* **121**, 187401 (2018).
32. M. Hirschberger, J. W. Krizan, R. J. Cava, N. P. Ong, Large thermal Hall conductivity of neutral spin excitations in a frustrated quantum magnet. *Science* **348**, 106-109 (2015).
33. Y. Kasahara *et al.*, Anomalous quasiparticle transport and superclean superconducting state of CeCoIn5. *Journal of Magnetism and Magnetic Materials* **310**, 569-571 (2007).
34. G. Zheng *et al.*, Transport evidence for the three-dimensional Dirac semimetal phase in ZrTe5. *Phys. Rev. B* **93**, 115414 (2016).
35. W. Wang *et al.*, Evidence for Layered Quantized Transport in Dirac Semimetal ZrTe5.

- Scientific Reports* **8**, 5125 (2018).
36. P. Yang *et al.*, Quantum Oscillations from Nontrivial States in Quasi-Two-Dimensional Dirac Semimetal ZrTe5 Nanowires. *Scientific Reports* **9**, 3558 (2019).
  37. P. B. Littlewood, The crystal structure of IV-VI compounds. I. Classification and description. *Journal of Physics C: Solid State Physics* **13**, 4855-4873 (1980).
  38. K. Behnia, Finding merit in dividing neighbors. *Science* **351**, 124 (2016).
  39. C. Fu *et al.*, Largely Suppressed Magneto-Thermal Conductivity and Enhanced Magneto-Thermoelectric Properties in PtSn4. *Research* **2020**, 4643507 (2020).
  40. J. Crossno *et al.*, Observation of the Dirac fluid and the breakdown of the Wiedemann-Franz law in graphene. *Science* **351**, 1058-1061 (2016).
  41. Q. Li *et al.*, Chiral magnetic effect in ZrTe5. *Nat Phys* **12**, 550 (2016).
  42. W. Zhang *et al.*, Observation of a thermoelectric Hall plateau in the extreme quantum limit. *Nature Communications* **11**, 1046 (2020).

## Figures

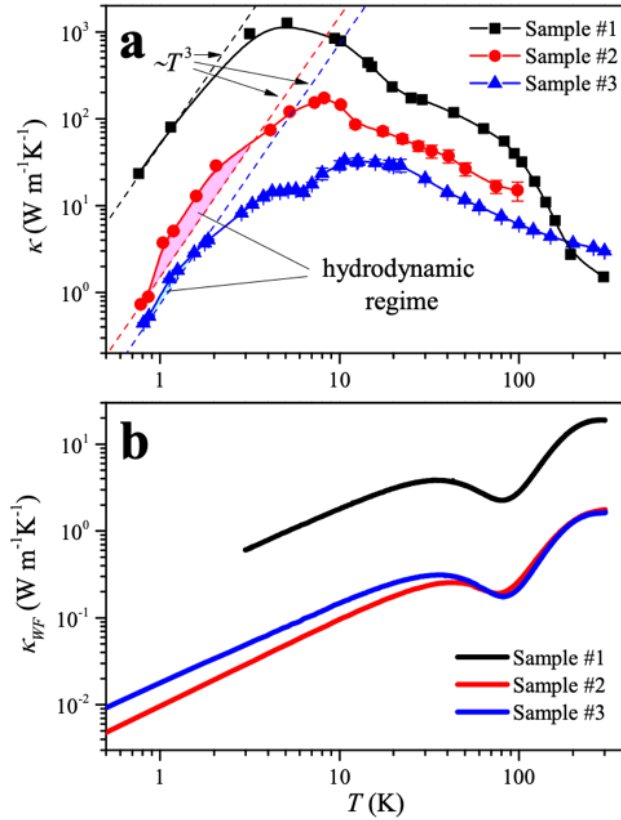


**Figure 1. (a)** Thermal conductivity as a function of temperature in a log-log plot in three different ZrTe<sub>5</sub> samples. The squares (Sample #1), circles (Sample #2) and triangles (Sample #3) indicate the total thermal conductivity. All the dash-lines are proportional to  $T^3$ . In Sample #2 and #3, the shaded regions denote that faster evolution of thermal conductivity rather than  $T^3$ -dependence. **(b)** Temperature-dependent charge carrier thermal conductivity  $\kappa_{WF}$ , which is calculated according to the Wiedemann-Franz law ( $\kappa_{WF} = \frac{T}{\rho} L_0$ , where the Lorenz number  $L_0 = 2.44 \times 10^{-8} \text{ W}\Omega\text{K}^{-2}$ ).

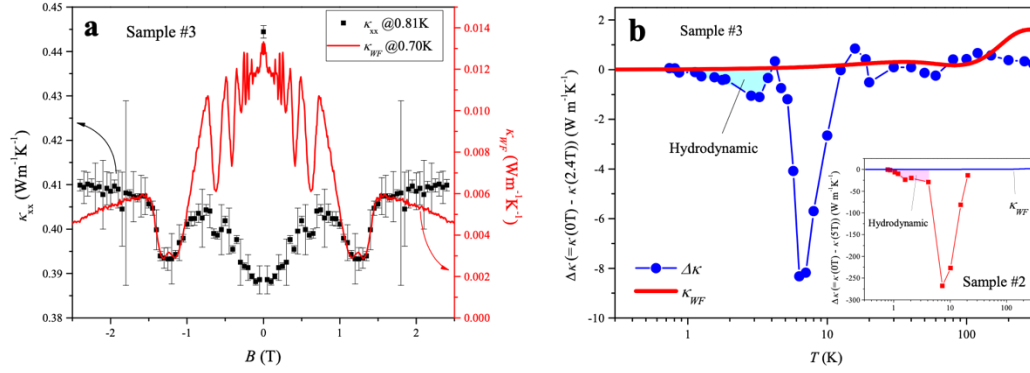


**Figure 2.** (a) Longitudinal total thermal conductivity  $\kappa_{xx}$  (closed squares) and electronically contributed thermal conductivity  $\kappa_{WF}$  (red-solid line) as a function of magnetic fields. The data was taken at  $T = 0.81$  K ( $\kappa_{xx}$ ) and  $T = 0.70$  K ( $\kappa_{WF}$ ), respectively. (b) Extracted charged quasiparticles contribution to the thermal conductivity of Sample #3 (closed circle). Sample #2 result is represented in the inset of (b). Both samples show the deviation of  $\Delta\kappa$  in a hydrodynamic regime as shaded. See main text for details.

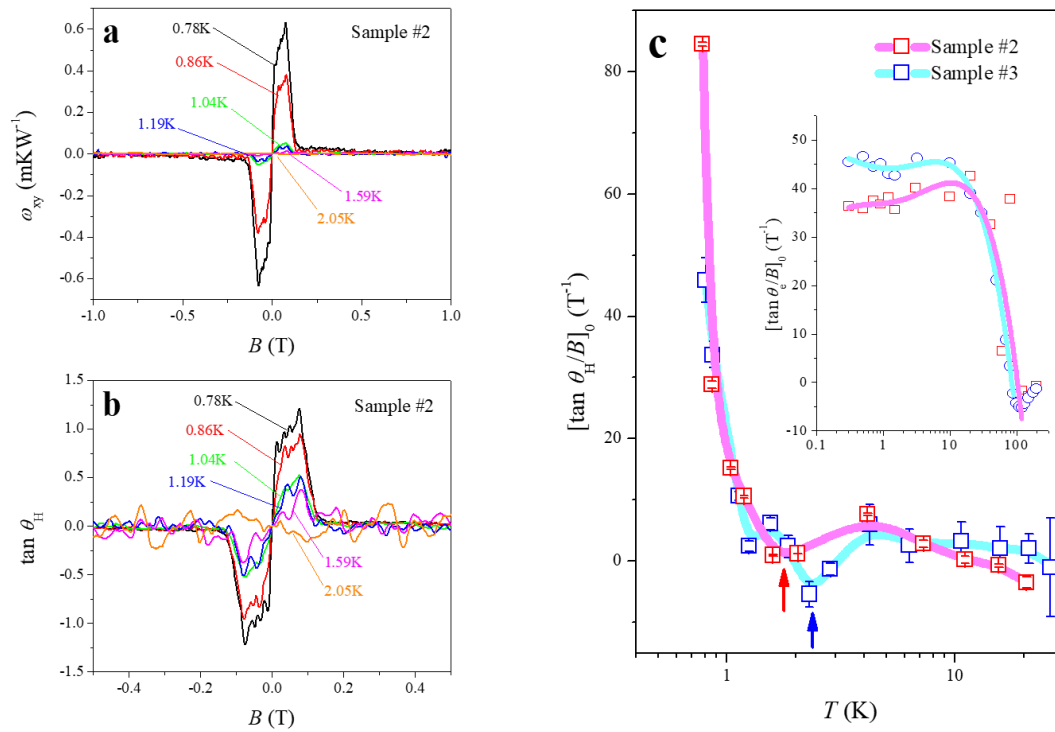


**Figure 3.** (a) Magnetic field dependence of the thermal Hall resistivity  $\omega_{xy}$  at various temperatures on Sample #2. (b) Tangential Hall angle ( $\tan \theta_H = \frac{\kappa_{xy}}{\kappa_{xx}}$ ) in a magnetic field range of -0.5 to 0.5 T at different temperatures on Sample #2. (c) Temperature-dependent slope of  $\tan \theta_H/B$  in the zero-magnetic-field-limit for both Sample #2 and #3. In general, this quantity is proportional to the mean-free-path of the quasiparticles. The vertical arrows denote the local minima. The inset of (c) presents the initial slope of the electronic Hall angle.

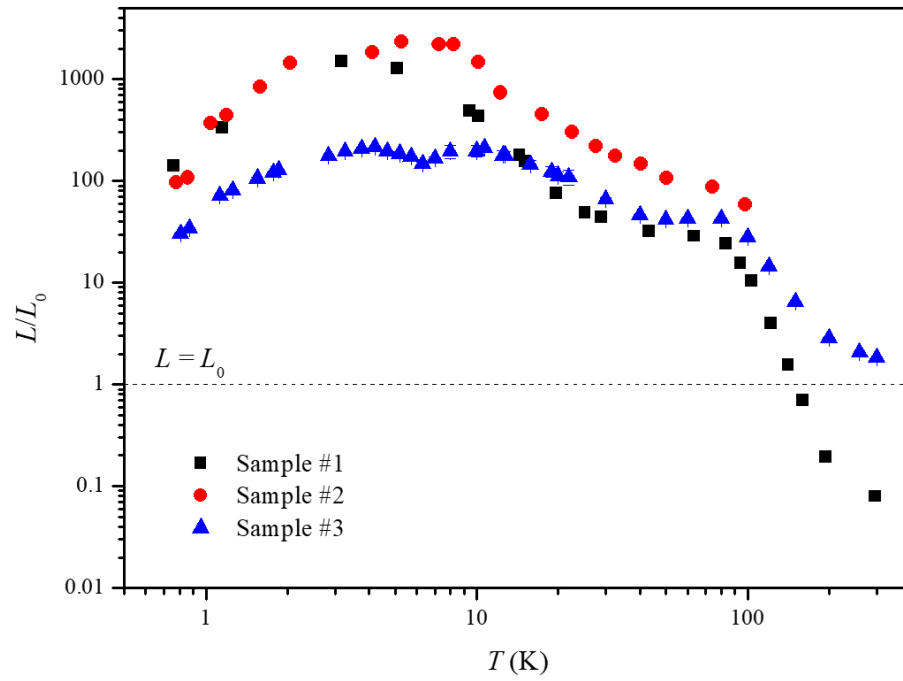


**Figure 4.** Temperature dependence of Lorenz ratio ( $L/L_0$ ) for ZrTe<sub>5</sub> single crystals used in this study. Horizontal line (dotted) is a guideline when  $L=L_0$ .